Disorder-induced temperature-dependent transport in graphene: Puddles, impurities, activation, and diffusion

Qiuzi Li, E. H. Hwang, and S. Das Sarma
Condensed Matter Theory Center, Department of Physics, University of Maryland, College Park, Maryland 20742, USA
(Received 12 May 2011; published 23 September 2011)

We theoretically study the transport properties of both monolayer and bilayer graphene in the presence of electron-hole puddles induced by charged impurities that are invariably present in the graphene environment. We calculate the graphene conductivity by taking into account the non-mean-field two-component nature of transport in the highly inhomogeneous density and potential landscape, where activated transport across the potential fluctuations in the puddle regimes coexists with regular metallic diffusive transport. The existence of puddles allows the local activation at low carrier densities, giving rise to an insulating temperature dependence in the conductivity of both monolayer and bilayer graphene systems. We also critically study the qualitative similarity and the quantitative difference between monolayer and bilayer graphene transport in the presence of puddles. Our theoretical calculation explains the nonmonotonic feature of the temperature-dependent transport, which is experimentally generically observed in low mobility graphene samples. We establish the two-component nature (i.e., both activated and diffusive) of graphene transport arising from the existence of potential fluctuation induced inhomogeneous density puddles. The temperature dependence of the graphene conductivity arises from many competing mechanisms, even without considering any phonon effects, such as thermal excitation of carriers from the valence band to the conduction band, temperature-dependent screening, thermal activation across the potential fluctuations associated with the electron-hole puddles induced by the random charged impurities in the environment, leading to very complex temperature dependence, which depends both on the carrier density and the temperature range of interest.

DOI: 10.1103/PhysRevB.84.115442 PACS number(s): 72.80.Vp, 72.10.−d, 73.22.Pr, 81.05.ue

I. INTRODUCTION

Graphene, as a novel gapless two dimensional (2D) chiral electron-hole system, has attracted great interest in recent years, both experimentally and theoretically.[1,2] Its transport properties have been at the center of key fundamental and technological efforts with vast potential for applications in future nanotechnology.[3] For monolayer graphene (MLG), the fundamental interest arises from its unique linear chiral Dirac carrier dispersion with a zero energy gap between conduction and valence band.[4] The bilayer graphene (BLG) is also intriguing as its physical properties lie between MLG and 2D semiconductor-based electron gas (2DEG) systems, which are gapped and nonchiral with a quadratic band dispersion. Much of the early work on graphene transport focused on the density-dependent (i.e., gate voltage tuned)[1,4–8] and temperature-dependent[1,9–12] conductivity in homogeneous MLG and BLG systems. The basic graphene transport properties, particularly at high densities far from the charge neutral Dirac point, are now reasonably well understood.[1]

However, unintended charged impurities, which are invariably present in the graphene environment, (e.g., the substrate-graphene interface), lead to the formation of inhomogeneous electron-hole puddles in the system,[13,14] which have been confirmed by experiments[15,16] using the techniques of scanning potential and tunneling microscopies. Although MLG samples show a metallic behavior at high densities a weak "insulating" temperature-dependent conductivity $\sigma(T)$ has been measured at low carrier density and at the charge neutrality point (CNP).[9] [We define insulating/metallic temperature dependence of conductivity $\sigma(T)$ as $d\sigma(T)/dT$ being positive/negative at fixed gate voltage.] In addition, a recent experiment[17] on low mobility MLG grown by chemical vapor deposition (CVD) shows a strong insulating behavior at low temperatures and a metallic feature at high temperatures manifesting a nonmonotonic temperature dependence in the measured electrical conductivity. In BLG samples[18–21] the strong insulating behavior in the temperature-dependent conductivity has been observed not only near CNP but also at carrier densities as high as 10^{12} cm^{-2} or higher. To be more specific, in Ref. 18, $\sigma(T)$ in BLG increases by 20–40% as temperature T increases from 4–300 K for carrier density in the range 3.19×10^{12} to 7.16×10^{12} cm^{-2}. To understand this anomalous temperature dependence in $\sigma(T)$, both MLG and BLG, it is essential to know the role of disorder in graphene transport. We note that phonon scattering (Refs. 22 and 23), although being weak in graphene, always contributes an increasing resistivity with increasing temperature and thus always leads to metallic behavior, and thus cannot be the mechanism for the intriguing insulating temperature dependence often observed in graphene transport at lower carrier densities—in fact, at very high temperatures (>300 K) graphene should always manifest metallic temperature dependence in its conductivity due to phonon-scattering effects, which we would ignore in the current work. Our goal here is to theoretically study in a comprehensive manner the temperature dependence of graphene transport properties arising entirely from the disorder effects.

The experimentally measured anomalous temperature-dependent conductivity of BLG has been theoretically investigated by applying the analytic statistical theory to the inhomogeneous potential fluctuation and it is found that the anomalous BLG $\sigma(T)$ is likely to be caused by the electron-hole puddles induced by randomly distributed disorder in the graphene environment.[24] In this paper, we extend this work and apply the same analytic statistical theory to MLG systems

and explain the intriguing coexistence of both metallic and insulating features of MLG $\sigma(T)$. In the presence of large fluctuating potentials $V(\mathbf{r})$ associated with microscopic configurations of Coulomb disorder in the system, the local Fermi level, $\mu(\mathbf{r}) = E_F - V(\mathbf{r})$, would necessarily have large spatial fluctuations. We carry out an analytical theory implementing this physical idea by assuming that the value of the potential at any given point follows a Gaussian distribution, parametrized by $s = V_{\rm rms}$ [the root-mean-square fluctuations or the standard deviation in $V(\mathbf{r})$ about the average potential]. This distribution can then be used to average the local density of states to obtain effective carrier densities, which can then be used to compute the physical quantities of interest.[25] The observed anomalous temperature-dependent $\sigma(T)$ is then understood as the competition between the thermal activation of carrier density and temperature-dependent screening effects. Our theory explains the suppression of the insulating behavior in higher mobility samples with lower disorder, which is consistent with experimental observations. We also provide the similarity and the quantitative difference between monolayer and bilayer graphene transport in the presence of puddles.

The motivation of our theory comes from the observation that the electron-hole puddles, which dominate the low-density graphene landscape, allow for a two-component semiclassical transport behavior, where the usual metallic diffusive carrier transport is accompanied by transport by activated carriers that have been locally thermally excited above the potential fluctuations imposed by the static disorder. This naturally allows for both insulating and metallic transport behavior occurring preferentially respectively at lower and higher carrier densities since the puddles disappear with increasing carrier density due to screening. At zero temperature (where no activation is allowed) or at very high carrier density (where puddles are suppressed), only diffusive transport is possible. But at any finite temperatures and at not too high densities, there would always be a two-component transport with both activated and diffusive carriers contributing to conductivity. Our theory develops this idea into a concrete description. We emphasize that our theory explicitly takes into account the inhomogeneous nature of the graphene landscape and is non-mean-field as a matter of principle.

This paper is organized as follows. In Sec. II, we introduce the analytical statistical theory to describe random electronic potential fluctuations created by charged impurities in the environment. We also calculate the modified density of states and the corresponding temperature-dependent effective carrier density in monolayer graphene. Then, in Sec. III, we describe the calculations and the main features of the temperature-dependent conductivity of MLG in the presence of density inhomogeneity. In Secs. IV and V, we elaborate and extend our earlier results for the interplay between density inhomogeneity and temperature in bilayer graphene (BLG) transport. We further discuss the connection of our theory to earlier theories in Sec. VI. We discuss the similarities and quantitative differences among the effects of inhomogeneity (i.e., the puddles) on MLG and BLG transport and summarize our results in Sec. VII. In the Appendix, we discuss a microscopic theory to calculate the effects of potential fluctuation on graphene systems, providing a self-consistent formulation of graphene density of states in the presence of random charged impurities near the graphene/substrate interface, showing in the process that this microscopically calculated density of states agrees well with the model density of states obtained from the Gaussian fluctuations.

II. TEMPERATURE-DEPENDENT CARRIER DENSITY FOR INHOMOGENEOUS MLG

It is well known that MLG breaks up into an inhomogeneous landscape of electron-hole puddles, especially around the charge neutral point (CNP).[15,16,26] Below we derive an analytic statistical theory taking account of the effects of inhomogeneous density in monolayer graphene (MLG) to explain the nonmonotonic temperature-dependent transport observed in MLG.[9,17] We start by assuming that charged impurities, located in the substrate or near the graphene, create a local electrostatic potential, which fluctuates randomly about its average value across the surface of the graphene sheet. The potential fluctuations themselves are assumed to be described by a statistical distribution function $P(V)$ where $V = V(\mathbf{r})$ is the fluctuating potential energy at the point $\mathbf{r} \equiv (x,y)$ in the 2D MLG plane. We approximate the probability $P(V)dV$ of finding the local electronic potential energy within a range dV about V to be a Gaussian form, i.e.,

$$P(V) = \frac{1}{\sqrt{2\pi s^2}} \exp(-V^2/2s^2), \tag{1}$$

where s is the standard deviation (or equivalently, the strength of the potential fluctuation), which is used as an adjustable parameter to tune the tail width.[27] In the Appendix, we provide a microscopic approach to self-consistently solve the strength of potential fluctuations in the presence of charged impurities. Due to the electron-hole symmetry in the problem, we only provide the formalism and equations for electronlike carriers and the hole part can be obtained simply by changing E to $-E$.

The potential fluctuations given by Eq. (1) affect the overall electronic density of states (DOS) in MLG. In our model we do not assume the size of the puddles to be identical, but we take the puddle sizes to be completely random controlled by the distribution function given in Eq. (1). We emphasize that our assumption of a Gaussian distribution for the potential fluctuations, equivalently implying a Gaussian distribution for the density fluctuations associated with the puddles, is known to be an excellent quantitative approximation to the actual numerically calculated puddle structures in graphene.[1,26] The characteristics of the puddles are determined by both the sign and the magnitude of $V - E_F$, i.e., a negative (positive) $V - E_F$ indicates an electron (hole) region. A different approach utilizing equal size puddles with a certain potential V has been used to calculate transport coefficients using a numerical transfer-matrix technique.[28] Then in the presence of electron-hole puddles the density of states is increased by the allowed electron region fraction and given by[27,29,30]

$$\begin{aligned} D_e(E) &= \int_{-\infty}^{E} \frac{g_s g_v (E-V)}{2\pi(\hbar v_F)^2} P(V) dV \\ &= D_1 \left[\frac{E}{2} \mathrm{erfc}\left(-\frac{E}{\sqrt{2}s}\right) + \frac{s}{\sqrt{2\pi}} \exp\left(-\frac{E^2}{2s^2}\right) \right], \end{aligned} \tag{2}$$

where erfc(x) is the complementary error function,

$$\mathrm{erfc}(x) = \frac{2}{\sqrt{\pi}} \int_x^\infty e^{-t^2} dt, \tag{3}$$

and $D_1 = \frac{g_s g_v}{2\pi(\hbar v_F)^2}$, where v_F is the graphene Fermi velocity, $g_s = 2$ and $g_v = 2$ are the spin and valley degeneracies, respectively. We have $D_1 = 1.5 \times 10^8$ cm^{-2}/meV^2 with the Fermi velocity $v_F = 10^6$ m/s. Note that the tail of the DOS is determined by the potential fluctuation strength s. For the case $s = 0$, the system becomes homogeneous and $D_e(E) = D_1 E$. In this case there is no carrier density at the Dirac point ($E = 0$) at zero temperature. It is apparent that in the presence of potential fluctuations, the $D_e(E)$ starts at finite value $\frac{D_1 s}{\sqrt{2\pi}}$ at $E = 0$ and approaches $D_1 E$ in high-energy limit. For the high-energy limit, the carrier is essentially free since nearly every point of the system is accessible. In Fig. 1, we show the normalized density of states as a function of energy for both electrons and holes in MLG. We mention that the self-consistent microscopic theory gives the same structure for the density of states of graphene systems (see the Appendix).

Since monolayer graphene is a semimetal or zero-gap semiconductor, the electron density at finite temperatures increases due to the direct thermal excitation from valence band to conduction band, which is one of the important sources of temperature-dependent transport at low carrier densities. Therefore we first consider the temperature dependence of thermally excited electron density. The total electron density is given by

$$n_e = \int_{-\infty}^{\infty} D_e(E) \frac{dE}{e^{\beta(E-\mu)} + 1}, \tag{4}$$

where $\beta = 1/k_B T$ and μ is the chemical potential. At $T = 0$, μ becomes the Fermi energy $\mu(T = 0) = E_F$.

A. $n_e(T)$ of MLG at CNP ($E_F = 0$)

When the Fermi energy is zero (or at CNP) all electrons are located in the band tail at $T = 0$ and the electron and hole densities in the band tail are given by

$$n_0 = n_e(E_F = 0) = n_h(E_F = 0) = D_1 \frac{s^2}{4}. \tag{5}$$

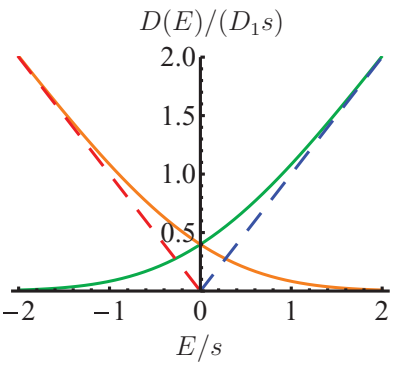

FIG. 1. (Color online) Normalized density of states for both electron and hole in MLG. The solid and dashed lines are for the DOS in inhomogeneous and homogeneous systems, respectively. The electron (hole) band tail locates at $E < 0$ ($E > 0$), which gives rise to electron (hole) puddles at $E < 0$ and $E > 0$.

Note that the electron (or hole) density in the band tails increases quadratically with the standard deviation s. At finite temperatures the behavior of $n_e(T)$ at CNP becomes

$$n_e(T) = n_0 \left[1 + \frac{\pi^2}{3} \left(\frac{k_B T}{s} \right)^2 \right]. \tag{6}$$

The leading-order temperature dependence in $n_e(T)$ is quadratic. For homogeneous MLG ($s = 0$) with the linear-in-energy behavior of the DOS, the electron density is given by $n_e(T) = \frac{D_1 \pi^2}{12} k_B^2 T^2$. In particular, in the ballistic regime the number of propagating channels increases due to the thermal smearing of the Fermi surface, which leads to the observation of an insulating behavior in $\sigma(T)$ at CNP for high mobility suspended graphene samples.[31–33] The presence of the band tail does not change the quadratic temperature dependence in the thermal excitation when the system is at the charge neutral point ($E_F = 0$). But the inhomogeneous MLG has n_0 electrons in the band tails. In Fig. 2(a) we show the temperature-dependent electron density at CNP for different values of standard deviation s.

B. $n_e(T)$ of MLG at finite doping ($E_F > 0$)

In the case of finite doping (or gate voltage), i.e., $E_F \neq 0$, the electron density of the homogeneous MLG (i.e., $s = 0$) is given by

$$\begin{aligned} n_{0e}(T) &= D_1 \int_0^\infty \frac{E dE}{\exp[\beta(E - \mu_0)] + 1} \\ &= -D_1 \frac{F_1(\mu_0 \beta)}{\beta^2}, \end{aligned} \tag{7}$$

where $F_1(x) = \int_0^\infty \frac{t\, dt}{1+\exp(t-x)}$, and μ_0 is the chemical potential of homogeneous MLG and is determined by the conservation of the total electron density. Then the chemical potential is given by the relation $\frac{E_F^2 \beta^2}{2} = F_1(\beta\mu_0) - F_1(-\beta\mu_0)$. Using the asymptotic forms[11] of the function $F_1(x)$ for $x \ll 1$ and $x \gg 1$, i.e.,

$$\begin{aligned} F_1(x) &\approx \frac{\pi^2}{12} + x \ln 2 + \frac{x^2}{4} \quad \text{for } |x| \ll 1, \\ F_1(x) &\approx \left[\frac{x^2}{2} + \frac{\pi^2}{6} \right] \theta(x) + x \ln(1 + e^{-|x|}) \text{ for } |x| \gg 1, \end{aligned} \tag{8}$$

we have the asymptotic formula for the chemical potential in both low- and high-temperature limits for homogeneous MLG,

$$\begin{aligned} \mu_0(T) &\simeq E_F \left[1 - \frac{\pi^2}{6} \left(\frac{T}{T_F} \right)^2 \right] \quad \text{for } T \ll T_F \\ \mu_0(T) &\simeq \frac{E_F}{4 \ln 2} \frac{T_F}{T} \quad \text{for } T \gg T_F. \end{aligned} \tag{9}$$

Then the corresponding asymptotic formula of the electron density [Eq. (7)] are given by

$$\begin{aligned} n_{0e}(T) &\simeq \frac{D_1 E_F^2}{2} \left(1 + \frac{\pi^4}{36} \frac{T^4}{T_F^4} \right) \quad \text{for } T \ll T_F, \\ n_{0e}(T) &\simeq \frac{D_1 E_F^2 \pi^2}{12} \frac{T^2}{T_F^2} \quad \text{for } T \gg T_F. \end{aligned} \tag{10}$$

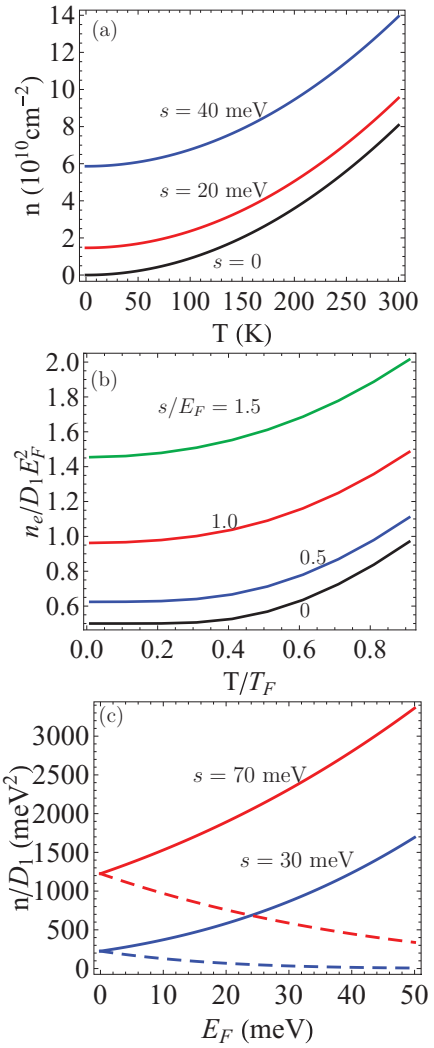

FIG. 2. (Color online) (a) Electron density of MLG at CNP as a function of temperature for different s. At $T = 0$ the density is given by $n_0 = D_1 s^2/4$. (b) Temperature-dependent electron density of MLG at finite E_F for different s. For $s/E_F \neq 0$ the leading-order behavior is quadratic. (c) Total electron densities (solid lines) and hole densities (dashed lines) of MLG as a function of E_F for two different $s = 30$ and 70 meV. The densities at the band tails are given by $n_e(E_F = 0) = n_h(E_F = 0) = D_1 s^2/4$.

Since the direct thermal excitation is suppressed due to the finite Fermi energy, the excited electron density at low temperatures ($T \ll T_F$) increases quartically rather than quadratically. But at high temperatures ($T \gg T_F$), the total electron density becomes a quadratic function of temperature as shown for an undoped MLG.

Next, we derive the temperature dependence of thermally excited electron density in the presence of electron-hole puddles ($s \neq 0$) at finite doping ($E_F \neq 0$). At zero temperature the electron density for the inhomogeneous MLG can be written as

$$n_e(0) = \frac{D_1 E_F^2}{4}\left[(1+\tilde{s}^2)\mathrm{erfc}\left(-\frac{1}{\sqrt{2}\tilde{s}}\right) + \sqrt{\frac{2}{\pi}}\tilde{s}\exp\left(-\frac{1}{2\tilde{s}^2}\right)\right],$$

$$n_h(0) = \frac{D_1 E_F^2}{4}\left[(1+\tilde{s}^2)\mathrm{erfc}\left(\frac{1}{\sqrt{2}\tilde{s}}\right) - \sqrt{\frac{2}{\pi}}\tilde{s}\exp\left(-\frac{1}{2\tilde{s}^2}\right)\right], \quad (11)$$

where $\tilde{s} = s/E_F$. The presence of electron-hole puddles does not induce any additional charge in the MLG system and the net carrier density $n = n_e - n_h$ should be conserved. Then, the finite-temperature chemical potential $\mu(T)$ changes as a function of both temperature and the strength of potential fluctuation s, and it should satisfy the following relation:

$$\int_{-\infty}^{E_F} D_e(E)dE - \int_{E_F}^{\infty} D_h(E)dE = \int_{-\infty}^{\infty} \frac{D_e(E)dE}{1+\exp[\beta(E-\mu)]} - \int_{-\infty}^{\infty} \frac{D_h(E)dE}{1+\exp[\beta(\mu-E)]}, \quad (12)$$

where $D_e(E)$ is the electronic density of states given by Eq. (2) and $D_h(E) = D_e(-E)$ is the density of states for holes. The asymptotic analytical formula of the chemical potential $\mu(T)$ for inhomogeneous MLG is obtained as

$$\mu(T) \simeq E_F\left[1 - \frac{\pi^2}{6}\left(\frac{T}{T_F}\right)^2 A(\tilde{s})\right] \quad \text{for} \quad T \ll T_F,$$
$$\mu(T) \simeq E_F B(\tilde{s},t) \quad \text{for} \quad T \gg T_F, \quad (13)$$

where functions $A(\tilde{s})$ and $B(\tilde{s})$ are given as follows:

$$A(\tilde{s}) = e^{1/2\tilde{s}^2}\mathrm{erf}\left[\frac{1}{\sqrt{2}\tilde{s}}\right] \Big/ \left(\sqrt{\frac{2}{\pi}}\tilde{s} + e^{1/2\tilde{s}^2}\mathrm{erf}\left[\frac{1}{\sqrt{2}\tilde{s}}\right]\right)$$
$$B(\tilde{s},t) = \left(\frac{e^{-1/2\tilde{s}^2}\tilde{s}}{\sqrt{2\pi}} + \frac{1}{2}(\tilde{s}^2+1)\mathrm{erf}\left[\frac{1}{\sqrt{2}\tilde{s}}\right]\right) \Big/ \left(2\ln 2\, t + \frac{\tilde{s}^2}{4t}\right), \quad (14)$$

where $t = T/T_F$ and $\mathrm{erf}(x) = \frac{2}{\sqrt{\pi}}\int_0^x e^{-t^2}dt$ is the error function.

Combining Eqs. (2), (4), and (13), we obtain the asymptotic analytical formula of the electron density for inhomogeneous MLG at low- and high-temperature limits as

$$n_e(T) \simeq n_e(0) + D_1 E_F^2 \frac{\pi^2}{12}\frac{T^2}{T_F^2}[1 - A(\tilde{s})] \quad \text{for} \quad T \ll T_F,$$
$$n_e(T) \simeq n_{0e}(T) + n_e(0) - \frac{D_1 E_F^2}{4} \quad \text{for} \quad T \gg T_F. \quad (15)$$

In the low-temperature limit ($T \ll T_F$), the leading-order term for the electron density has the same quadratic behavior as in undoped homogeneous MLG ($E_F = 0$), but the coefficient is strongly suppressed by fluctuation for the case of $s < E_F$, i.e., the high carrier density sample. While in the case of $s > E_F$, i.e., the low carrier density sample, the existence of electron-hole puddles gives rise to a notable quadratic behavior for electron density $n_e(T)$ [see Fig. 2(b)].

III. CONDUCTIVITY OF INHOMOGENEOUS MLG

In this section, we calculate the finite-temperature conductivity for inhomogeneous MLG with the temperature-dependent effective carrier density derived above. The exis-

tence of electron-hole puddles allows that the current flows through "percolation channels" and the transport properties of the inhomogeneous MLG system can be derived using the self-consistent effective-medium theory of conductance in composite mixtures,[34] where the number of electrons per puddle is not an important issue for our theory. The percolation assumption is valid as long as the potential fluctuation is larger than the thermal energy of the carriers. Otherwise transport due to disorder scattering dominates. We emphasize that in our formalism the crossover from the percolation transport to ordinary scattering-dominated diffusive transport is guaranteed as the temperature is increased since we are explicitly taking into account both diffusive transport of free carriers and activated transport of the classically localized carriers in our theory. The only effects we neglect are quantum tunneling through the potential barriers and quantum interference since ours is a semiclassical theory. We also do not consider Klein tunneling explicitly in this paper because the Klein tunneling occurs at zero temperature for normal incident carriers at the electron-hole puddle boundary. We also apply the Boltzmann transport theory, where we include the scattering mechanism with screened Coulomb impurities and short-range disorder.[11] Note that the application of Boltzmann transport theory is justifiable because the quantum interference effects are not experimentally observed in the temperature regime of interest to us in this work. It is conceivable that quantum interference and localization play some roles in graphene transport at very low temperatures, which is beyond the scope of this paper. We also neglect all phonon effects in this work since electron-phonon coupling is weak in graphene. Phonon effects are relevant at high temperatures (>100 K) and have been considered in the literature.[22,23]

At CNP ($E_F = 0$) electrons and holes are equally occupied. As the Fermi energy increases, more electrons occupy an increasingly larger proportion of space. As the Fermi energy increases to $E_F \gg s$, nearly all space is populated by the electrons [see Fig. 2(c)] and the conductivity of the system approaches the characteristic of the homogeneous material. Thus there is a possible coexistence of metallic and thermally activated transport in the presence of electron-hole puddles. When electron puddles occupy more space than hole puddles, most electrons follow the continuous metallic paths extended throughout the system, but it is possible at finite temperatures that the thermally activated transport of electrons persists above the hole puddles. On the other hand, holes in hole puddles propagate freely, but when they meet electron puddles, activated holes conduct over the electron puddles. Carrier transport in each puddle is characterized by propagation of weak scattering transport theory.[34] The activated carrier transport of prohibited regions, where the local potential energy V is less (greater) than Fermi energy for electrons (holes), is proportional to the Fermi factor. If σ_e and σ_h are the average conductivity of electron and hole puddles, respectively, then the activated conductivities are given by

$$\sigma_e^{(a)}(V) = \sigma_e \exp[\beta(E_F - V)], \tag{16a}$$

$$\sigma_h^{(a)}(V) = \sigma_h \exp[\beta(V - E_F)], \tag{16b}$$

where the density- and temperature-dependent average conductivities (σ_e and σ_h) are given within the Boltzmann transport theory[1] by $\sigma_e \propto n_e\langle\tau\rangle$ and $\sigma_h \propto n_h\langle\tau\rangle$, where n_e and n_h are average electron and hole densities, respectively, and $\langle\tau\rangle$ is the average transport relaxation time, which includes the thermal smearing effects and depends explicitly on the scattering mechanism[1] and it is given by

$$\langle\tau\rangle = E_F \frac{\int d\epsilon D_e(\epsilon)\tau(\epsilon)(-\partial f/\partial\epsilon)}{\int d\epsilon D_e(\epsilon) f(\epsilon)}, \tag{17}$$

where $\tau(\epsilon)$ and $f = 1/(1 + e^{\beta(\epsilon-\mu)})$ are, respectively, the energy-dependent transport scattering time and the finite-temperature Fermi distribution function. Because the density inhomogeneity effects already been considered in the variation of effective carrier density, we use the DOS of homogeneous MLG $D_e(\epsilon) = D_1\epsilon$ in Eq. (17) to avoid double counting, and $\tau(\epsilon)$ is given by

$$\frac{\hbar}{\tau(\epsilon_{p\mathbf{k}})} = 2\pi n_{\rm dis} \int \frac{d^2k'}{(2\pi)^2} |\langle V_{p\mathbf{k},p\mathbf{k}'}\rangle|^2 g(\theta_{\mathbf{k}\mathbf{k}'}) \times[1 - \cos\theta_{\mathbf{k}\mathbf{k}'}]\delta(\epsilon_{p\mathbf{k}'} - \epsilon_{p\mathbf{k}}), \tag{18}$$

where $\epsilon_{p\mathbf{k}} = p\hbar v_F k$ is the carrier energy for the pseudospin state "p" and $\mathbf{k}$ is the 2D wave vector, $\langle V_{p\mathbf{k},p\mathbf{k}'}\rangle$ is the matrix element of the impurity disorder potential in the system environment, $\theta_{\mathbf{k}\mathbf{k}'}$ is the scattering angle between in- and out-wave vectors $\mathbf{k}$ and $\mathbf{k}'$, $g(\theta_{\mathbf{k}\mathbf{k}'}) = [1 + \cos\theta_{\mathbf{k}\mathbf{k}'}]/2$ is a wave function form factor associated with the chiral nature of MLG (and is determined by its band structure). $n_{\rm dis}$ is the appropriate 2D areal concentration of the impurity centers giving rise to the random disorder potential.[35] We consider two different kinds of disorder scattering mechanisms: (i) randomly distributed screened Coulomb disorder for which $n_{\rm dis}|\langle V_{p\mathbf{k},p\mathbf{k}'}\rangle|^2 = n_i|v_i(q)/\varepsilon(q)|^2$, where $v_i(q) = 2\pi e^2/(\kappa q)$ is the Fourier transform of the 2D Coulomb potential in an effective background lattice dielectric constant κ and $\varepsilon(q) \equiv \varepsilon(q,T)$ is the 2D finite-temperature static random-phase approximation (RPA) dielectric function[36] (note that we use n_i to denote the charged impurity density); (ii) short-range disorder for which $n_{\rm dis}|\langle V_{p\mathbf{k},p\mathbf{k}'}\rangle|^2 = n_d V_0^2$ where n_d is the 2D impurity density and V_0 is a constant short-range (i.e., a δ function in real space) potential strength. Note that the use of Born approximation for short-range disorder requires weak scattering condition,[37] which is verified by the disorder parameters we use in our calculation.

Now we denote the electron (hole) puddle as region "1" ("2"). In region 1 electrons occupy more space than holes when $E_F > 0$. The fraction of the total area occupied by electrons with Fermi energy E_F is given by $p = \int_{-\infty}^{E_F} P(V)dV$. Then the total conductivity of region 1 can be calculated,

$$\sigma_1 = \frac{1}{p}\int_{-\infty}^{E_F} (\sigma_e + \sigma_h^{(a)})P(V)dV = \sigma_e + \frac{\sigma_h}{2p} e^{\beta^2 s^2/2 - \beta E_F} \mathrm{erfc}\left(-\frac{E_F}{\sqrt{2}s} + \frac{\beta s}{\sqrt{2}}\right). \tag{19}$$

At the same time the holes occupy the area with a fraction $q = 1 - p$ and the total conductivity of region 2

becomes

$$\sigma_2 = \frac{1}{q}\int_{E_F}^{\infty}(\sigma_e^{(a)} + \sigma_h)P(V)dV$$
$$= \sigma_h + \frac{\sigma_e}{2q}e^{\beta^2 s^2/2+\beta E_F}\mathrm{erfc}\left(\frac{E_F}{\sqrt{2}s} + \frac{\beta s}{\sqrt{2}}\right). \quad (20)$$

The σ_1 and σ_2 are distributed according to the binary distribution. The conductivity of binary system can be calculated by using the effective-medium theory of conductance in mixtures.[34] The result for a 2D binary mixture of components with conductivity σ_1 and σ_2 is given by[34]

$$\sigma_t = \left(p - \frac{1}{2}\right)\left[(\sigma_1 - \sigma_2) + \sqrt{(\sigma_1 - \sigma_2)^2 + \frac{4\sigma_1\sigma_2}{(2p-1)^2}}\right]. \quad (21)$$

This result can be applied for all Fermi energy. For a large doping case, in which the hole puddles disappear, we have $p = 1$ and $\sigma_2 = 0$, then Eq. (21) becomes $\sigma = \sigma_1$, i.e., the conductivity of electrons in the homogeneous system.

A. $\sigma(T)$ of MLG at CNP ($E_F = 0$)

We first consider the conductivity at CNP ($E_F = 0$). The conductivities in each region are given by

$$\sigma_1 = \sigma_e\left[1 + \frac{\eta}{2p}e^{\beta^2 s^2/2}\mathrm{erfc}(\beta s/\sqrt{2})\right], \quad (22a)$$

$$\sigma_2 = \sigma_h\left[1 + \frac{1}{2q\eta}e^{\beta^2 s^2/2}\mathrm{erfc}(\beta s/\sqrt{2})\right], \quad (22b)$$

where $\eta = n_h/n_e$ is the ratio of the hole density to the electron density. Since the electrons and holes are equally populated, we have $p = q = 1/2$ and $\sigma_e = \sigma_h$, then the total conductivity becomes $\sigma_t = \sqrt{\sigma_1\sigma_2} = \sigma_1$. The asymptotic behavior of the conductivity at low temperatures ($k_B T \ll s$) becomes

$$\sigma_t(T) = \sigma_e\left[1 + \sqrt{\frac{2}{\pi}}\frac{k_B T}{s} - \frac{2}{\sqrt{\pi}}\frac{(k_B T)^3}{s^3}\right]. \quad (23)$$

The activated conductivity increases linearly with a slope $\sqrt{2/\pi}k_B/s$ as temperature increases. Typically s is smaller in higher mobility samples, which gives rise to stronger insulating behavior at low temperatures. The next order temperature correction to conductivity arises from the thermal excitation given in Eq. (6), which gives quadratic (T^2) temperature corrections. Thus in the low-temperature limit the total conductivity at the CNP is given by

$$\sigma_t = \sigma(0)\left[1 + \sqrt{\frac{2}{\pi}}\frac{k_B T}{s} + \frac{\pi^2}{3}\left(\frac{k_B T}{s}\right)^2\right]. \quad (24)$$

At high temperatures ($k_B T \gg s$) we have

$$\sigma_t = \sigma_e\left[2 - \sqrt{\frac{2}{\pi}}\frac{s}{k_B T} + \frac{s^2}{2(k_B T)^2}\right], \quad (25)$$

where the temperature dependence of σ_e has been given in Eq. (6). The total conductivity due to the activation behavior approaches a limiting value and all temperature dependence comes from the thermal excitation through the change of the effective carrier density in the presence of the inhomogeneity given in Eq. (6). Thus at very high temperatures ($T \gg s/k_B$) the MLG conductivity at the charge neutral point increases quadratically regardless of the sample quality. In Fig. 3 the temperature-dependent conductivity has been calculated at charge neutral point, where the temperature-dependent scattering mechanism can be neglected. In Ref. 17, about 60% increase of conductivity is observed as the temperature increases from 4 to 300 K. We estimate the potential fluctuation parameter $s \sim 80$ meV for this sample based on our theoretical analysis as compared with the data.

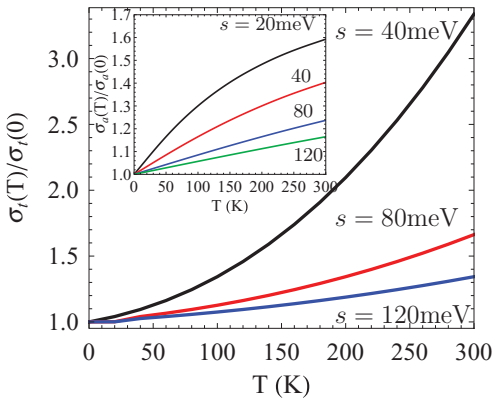

FIG. 3. (Color online) $\sigma_t(T)$ of MLG at charge neutral point for different s [Eq. (22a) and n_e as given in Eq. (6)]. Inset shows the thermally activated conductivity of MLG as a function of temperature, where $\sigma_a(T)/\sigma_a(0) = 1 + e^{\beta^2 s^2/2}\mathrm{erfc}(\beta s/\sqrt{2})$.

B. $\sigma(T)$ of MLG at finite doping ($E_F > 0$)

At finite doping ($E_F > 0$) the temperature-dependent conductivities are very complex because three energies (E_F, s, and $k_B T$) are competing among them. Especially when $k_B T \ll s$, regardless of E_F, we have the asymptotic behavior of conductivities in region 1 and 2 from Eqs. (19) and (20), respectively,

$$\sigma_1 = \sigma_e\left[1 + \frac{\eta}{2p}e^{-1/2\tilde{s}^2}\sqrt{\frac{2}{\pi}}\frac{1}{\tilde{s}/t - 1/\tilde{s}}\right], \quad (26a)$$

$$\sigma_2 = \sigma_h\left[1 + \frac{1}{2q\eta}e^{-1/2\tilde{s}^2}\sqrt{\frac{2}{\pi}}\frac{1}{\tilde{s}/t + 1/\tilde{s}}\right], \quad (26b)$$

where $\tilde{s} = s/E_F$ and $t = T/T_F$. The leading-order correction is linear but the coefficient is exponentially suppressed by the term $\exp(-E_F^2/2s^2)$. This fact indicates that in the high mobility sample with small s, the activated conductivity is weakly temperature dependent except at low-density regimes, i.e., $E_F < s$. Since the density increase by thermal excitation is also suppressed exponentially by the same factor [see Eq. (15)], the dominant temperature-dependent conductivity arises from the scattering time,[1] which manifests the metallic behavior. On the other hand, for a low mobility sample with a large s, the linear temperature dependence due to thermal activation can be observed even at high carrier densities $E_F \gtrsim s$.

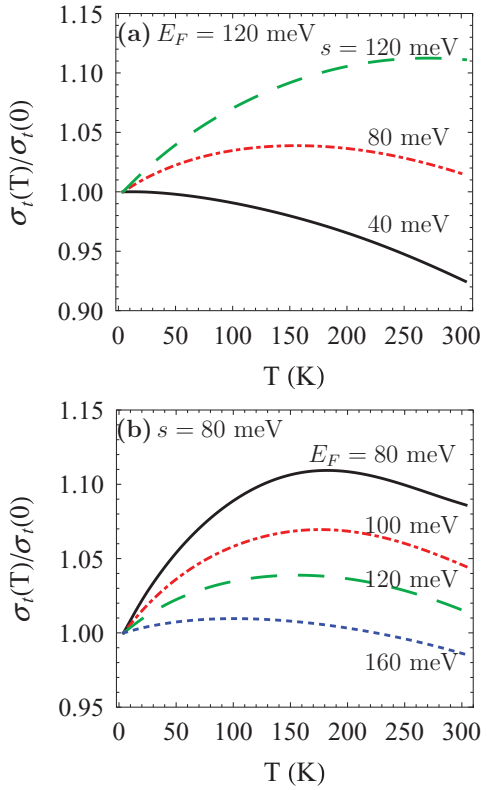

FIG. 4. (Color online) Calculated total conductivity $\sigma_t(T)/\sigma_t(0)$ of MLG with the following parameters: $n_i = 10^{12}$ cm^{-2} and $n_d V_0^2 = 2$ (eV Å)^2. (a) $\sigma_t(T)$ for $E_F = 120$ meV and for different s. (b) $\sigma_t(T)$ of MLG for $s = 80$ meV and for several $E_F = 80$, 100, 120, 160 meV, which correspond to the net carrier densities $n = n_e - n_h \simeq 0.9 \times 10^{12}$, 1.2×10^{12}, 1.5×10^{12}, and 2.3×10^{12} cm^{-2}.

In Fig. 4 we present the total conductivities of inhomogeneous MLG as a function of temperature (a) for a fixed Fermi energy and several s and (b) for a fixed s and several Fermi energies. The calculations for Fig. 4 are all carried out for MLG on SiO_2 substrate (corresponding to dielectric constant $\kappa \approx 2.5$), charged impurity density $n_i = 10^{12}$ cm^{-2}, and short-ranged disorder strength $n_d V_0^2 = 2$ (eV Å)^2. For total conductivity, the thermally activated insulting behavior competes with the temperature-dependent screening effects, where the latter always give the metallic behavior in conductivity for MLG samples. When s is small, the activated behavior is suppressed and the total conductivity shows the metallic behavior. While for large value of s, i.e., the low mobility sample, the thermal activation overwhelms the metallic temperature dependence and the system manifests insulating behavior. For $s \sim E_F$ the situation becomes much complex. At low temperatures, the leading order of the temperature dependence is linear [the second term in Eq. (26)] and the total conductivity starts at weakly insulating behavior. As the temperature increases, the screening effects begin to dominant leading to the metallic behavior. As a result, the temperature evolution of the conductivity becomes nonmonotonic and for large s (or low mobility samples) the nonmonotonic behavior can be more pronounced as shown in experiments.[17]

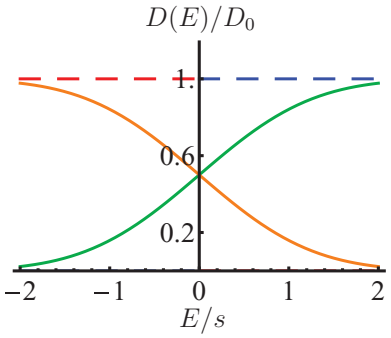

FIG. 5. (Color online) Normalized density of states for both electron and hole in BLG. The solid and dashed lines are for the DOS in inhomogeneous and homogeneous systems, respectively. The electron (hole) band tail locates at $E < 0$ ($E > 0$), which gives rise to electron (hole) puddles at $E < 0$ and $E > 0$.

IV. TEMPERATURE-DEPENDENT CARRIER DENSITY OF INHOMOGENEOUS BLG

In the following, we extend our previous study[24] on the insulating behavior in metallic bilayer graphene and compare it with MLG situation. The most important difference between MLG and BLG comes from the fact that, in the BLG, the two layers are weakly coupled by interlayer tunneling, leading to an approximately parabolic band dispersion with an effective mass about $m \simeq 0.033 m_e$ (m_e corresponds to the bare electron mass) in contrast to linear-dispersion Dirac carrier system for MLG. As done for MLG, we assume the electronic potential fluctuations in BLG system to be a Gaussian form given in Eq. (1) and this potential is felt equally by both layers.[25]

In the presence of potential fluctuations the density of states (DOS) for disordered BLG is given by $D_e(E) = \int_{-\infty}^{E} D_0 P(V) dV = D_0 \mathrm{erfc}(-E/\sqrt{2}s)/2$, where $D_0 = g_s g_v m/(2\pi\hbar^2)$ is the DOS in a homogeneous BLG system, where $g_s = 2$ and $g_v = 2$ are the spin and valley degeneracies, respectively. We have $D_0 = 2.8 \times 10^{10}$ cm^{-2}/meV assuming $m = 0.033 m_e$. The DOS of hole can be calculated from the following relation: $D_h(E) = D_e(-E)$. In Fig. 5, the density of states of both electron and hole are shown for the inhomogeneous BLG system. In the presence of potential fluctuations, the electron and hole coexist for certain amount of regions near CNP and their DOS approach to the homogeneous case as the carrier energy further increases.

Because BLG is also a gapless semiconductor like MLG, the direct thermal excitation from valence band to conduction band at finite temperatures composes an important source of temperature-dependent transport in BLG. Thus the temperature dependence of thermally excited electron density is first to be considered.

A. $n_e(T)$ of BLG at CNP ($E_F = 0$)

With the help of Eq. (4), we could get the total electron density for BLG in the presence of electron-hole puddles. We first consider the situation at CNP, where all electrons are located in the band tail at $T = 0$ and the electron density in the band tail is given by $n_0 = n_e(E_F = 0) = D_0 s/\sqrt{2\pi}$.[25] In contrast to the quadratic dependence of s in MLG, the electron

density in the band tail for BLG is linearly proportional to the standard deviation s. Unlike MLG, which has the exact formula for $n_0(T)$ [i.e., Eq. (6)], we could only find the asymptotic behavior of $n_0(T)$ at finite temperatures for BLG. The low-temperature ($k_BT/s \ll 1$) behavior of electron density at CNP becomes

$$n_e(T) = n_0\left[1 + \frac{\pi^2}{6}\left(\frac{k_BT}{s}\right)^2\right]. \tag{27}$$

Thus the electron density increases quadratically at the low-temperature limit. For homogeneous BLG with the constant DOS the electron density at finite temperatures is given by $n_e(T) = D_0 \ln(2) k_B T$, which has the universal slope $D_0 \ln(2) k_B$. The presence of the band tail suppresses the thermal excitation of electrons and gives rise to the quadratic behavior. However, at the high-temperature limit, the density increases linearly with the same slope approaching the homogeneous system, i.e.,

$$n(T) \sim D_0\left[\ln(2)k_BT + \frac{1}{8}\frac{s^2}{(k_BT)^2}\right]. \tag{28}$$

In Fig. 6(a) we show the temperature-dependent electron density at CNP for different standard deviations. Compared with the inset of Fig. 3, it is apparent that, even for the same strength of potential fluctuation s, the effects of thermal excitation of carrier density are much stronger in BLG than in MLG sample, which leads to more easily observed insulating behavior in BLG samples.

B. $n_e(T)$ of BLG at finite doping ($E_F > 0$)

In this subsection, we derived the total electron density at finite temperatures for inhomogeneous BLG away from CNP. Contrary to MLG, we need to calculate the finite-temperature chemical potential [i.e., Eqs. (9) and (13)]. The charge conservation relation in both homogeneous and inhomogeneous BLG gives the temperature-independent chemical potential $\mu \equiv E_F$, allowing us to directly calculate the total effective electron (hole) density. In the case of finite gate voltage, i.e., $E_F \neq 0$, the electron density of the homogeneous BLG for $s = 0$ is given by

$$n_{0e}(T) = D_0E_F[1 + t\ln(1 + e^{-1/t})], \tag{29}$$

where $t = T/T_F$ and $T_F = E_F/k_B$. The thermal excitation is exponentially suppressed due to the Fermi function at low temperatures ($T \ll T_F$). While at high temperatures ($T \gg T_F$) it increases linearly. In the presence of finite potential fluctuations ($s \neq 0$), the electron and hole density at zero temperature for the inhomogeneous system are given by

$$\begin{aligned} n_e(0) &= D_0E_F\left[\frac{1}{2}\mathrm{erfc}\left(\frac{-1}{\sqrt{2}\tilde{s}}\right) + \frac{\tilde{s}}{\sqrt{2\pi}}e^{-1/2\tilde{s}^2}\right], \\ n_h(0) &= D_0E_F\left[-\frac{1}{2}\mathrm{erfc}\left(\frac{1}{\sqrt{2}\tilde{s}}\right) + \frac{\tilde{s}}{\sqrt{2\pi}}e^{-1/2\tilde{s}^2}\right], \end{aligned} \tag{30}$$

where $\tilde{s} = s/E_F$ and the difference of electron and hole density ($n = n_e - n_h = D_0E_F$) is independent of the strength of potential fluctuation s [see Fig. 6(c)]. At low temperatures

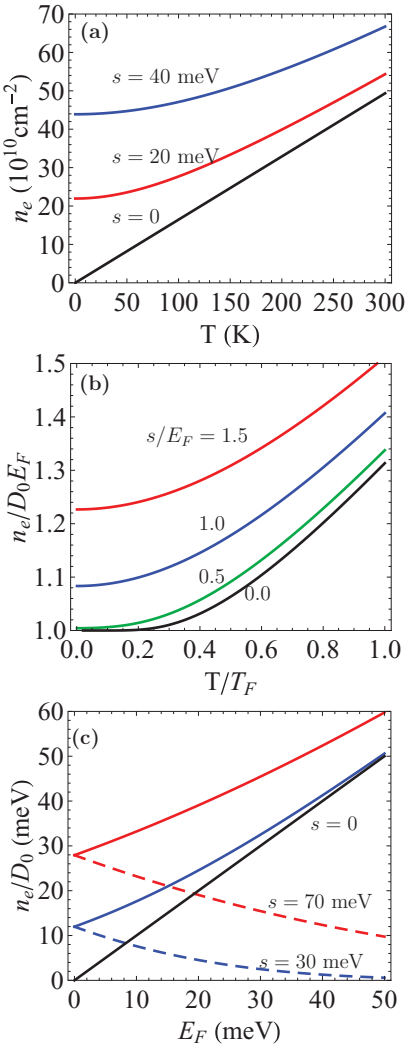

FIG. 6. (Color online) (a) Electron density of BLG at CNP as a function of temperature for different s. At $T = 0$ the density is given by $n_0 = D_0 s/\sqrt{2\pi}$. (b) Temperature-dependent electron density of BLG at finite E_F for different s. For $s/E_F \neq 0$ the leading-order behavior is quadratic while at $s = 0$ the density is exponentially suppressed. (c) Total electron densities (solid lines) and hole densities (dashed lines) of BLG as a function of E_F for two different $s = 30$ and 70 meV. The linear line represents the density difference $n = n_e - n_h = D_0E_F$, which linearly depends on the Fermi energy. The densities at the band tails are given by $n_e(E_F = 0) = n_h(E_F = 0) = D_0 s/\sqrt{2\pi}$.

($T \ll T_F$) the asymptotic behavior of the electron density is given by

$$n_e(T) = n_e(0) + D_0E_F\frac{\pi^2}{12\sqrt{2}}\frac{e^{-1/2\tilde{s}^2}}{\tilde{s}}\left(\frac{T}{T_F}\right)^2. \tag{31}$$

The leading-order quadratic behavior of $n_e(T)$ as in undoped BLG ($E_F = 0$) is strongly suppressed by potential fluctuation. For the situation $s > E_F$, the existence of electron-hole puddles gives rise to a notable quadratic behavior [see Fig. 6(b)]. At high temperatures ($T \gg T_F$) we find

$$n_e(T) = n_{0e}(T) + \frac{D_0E_F}{(1 + e^{\beta E_F})^2}\frac{\tilde{s}^2}{2}\frac{T_F}{T}, \tag{32}$$

where the linear temperature dependence of the electron density is dominant as the homogeneous system.

V. CONDUCTIVITY OF INHOMOGENEOUS BLG

With the help of total electron and hole density calculated above, we will derive the temperature-dependent conductivity for BLG in the presence of electron-hole puddles. We will apply both Boltzmann theory[35] and effective-medium theory[34] to interpret the intriguingly insulating behavior observed in BLG samples.[18,19,21]

The density- and temperature-dependent average conductivities in BLG, denoted as σ_e and σ_h, are given within the Boltzmann transport theory:

$$\sigma_e = \frac{n_e e^2 \langle \tau \rangle}{m},$$
$$\sigma_h = \frac{n_h e^2 \langle \tau \rangle}{m}, \tag{33}$$

where n_e and n_h are average electron and hole densities, respectively. $\langle \tau \rangle$ is the transport relaxation time for bilayer graphene,

$$\langle \tau \rangle = \frac{\int d\epsilon D_e(\epsilon)\epsilon\tau(\epsilon)(-\partial f/\partial\epsilon)}{\int d\epsilon D_e(\epsilon) f(\epsilon)}, \tag{34}$$

and $\tau(\epsilon)$ is calculated with Eq. (18). But for BLG systems, one needs to use the parabolic dispersion relation $\epsilon_{p\mathbf{k}} = p\hbar^2k^2/2m$ for the pseudospin state "p" and the static dielectric screening function derived in Ref. 38. The wave function form factor associated with the chiral nature of BLG is also different from the case in MLG, which is given by $g(\theta_{\mathbf{kk}'}) = [1 + \cos 2\theta_{\mathbf{kk}'}]/2$. To determine the average scattering time in BLG, we take into account the long-range charged impurity scattering and short-range defect scattering; it has been established that both contribute significantly to bilayer graphene transport properties.[35] The activated conductivities should also be included in the presence of density inhomogeneity in the BLG, which follow the same relation as given for MLG:

$$\sigma_e^{(a)}(V) = \sigma_e \exp[\beta(E_F - V)], \tag{35a}$$
$$\sigma_h^{(a)}(V) = \sigma_h \exp[\beta(V - E_F)]. \tag{35b}$$

A. $\sigma(T)$ of BLG at CNP

When electron-hole puddles form in the BLG samples [denote the electron (hole) puddle as region "1" ("2")], the transport properties can be treated with effective-medium theory as described in Sec. III, and Eqs. (19)–(23) for the inhomogeneous MLG also apply to the inhomogeneous BLG system. We will first discuss the total conductivity of BLG at CNP ($E_F = 0$). In this case, the electron and hole are equally occupied and the total conductivity $\sigma_t = \sigma_1$ [see Eqs. (22a) and (23)]. At the low-temperature limit ($T \ll s/k_B$), the activated conductivities increase linearly with a slope $\sqrt{2/\pi}k_B/s$ as the temperature increases. The next order temperature correction to the conductivity is quadratic T^2, which arises from the thermal activation [see Eq. (27)]. Thus at the low-temperature limit the total conductivity at CNP is given by

$$\sigma_t(T) = \sigma(0)\left[1 + \sqrt{\frac{2}{\pi}}\frac{k_BT}{s} + \frac{\pi^2}{6}\left(\frac{k_BT}{s}\right)^2\right]. \tag{36}$$

At high temperatures ($k_BT \gg s$), the total conductivity is given by

$$\sigma_t = \sigma_e\left[2 - \sqrt{\frac{2}{\pi}}\frac{s}{k_BT} + \frac{s^2}{2(k_BT)^2}\right]. \tag{37}$$

It is apparent that the activation behavior approaches a limiting value at the high-temperature limit ($T \gg s/k_B$) while the thermally activated electron density becomes dominant, which increases linearly with a universal slope ln(2) regardless of the sample quality. Thus all temperature dependence of the total conductivity comes from the thermal excitation through the change of the carrier density given in Eq. (28). In Fig. 7 we show the calculated temperature-dependent conductivity at the charge neutral point. The inset presents the activated conductivity versus the temperature. In Ref. 18, $\sigma_t(T)$ at the CNP of the BLG sample increases almost two times as temperature T varies from 4 to 300 K. Our theoretical analysis using a potential fluctuation parameter $s \sim 40$ meV gives reasonable agreement with the experimental data.

B. $\sigma(T)$ of BLG at finite doping ($E_F > 0$)

The temperature-dependent conductivities at finite doping ($E_F > 0$) are very complex because three energies (E_F, s, and k_BT) are competing. Regardless of E_F, when $k_BT \ll s$, we have the asymptotic behavior of conductivities in region 1 and 2 the same as the MLG situation, given in Eq. (26). But the average electron and hole conductivities (σ_e and σ_h) are quite different from MLG case, which is determined by the specific band dispersion relation and also the dielectric function $\epsilon(q,T)$. Thus the leading-order correction to σ_t in BLG is also linear, which comes from the activated conductivity, but the coefficient is exponentially suppressed by the term $\exp(-E_F^2/2s^2)$. In the high mobility sample with small s,

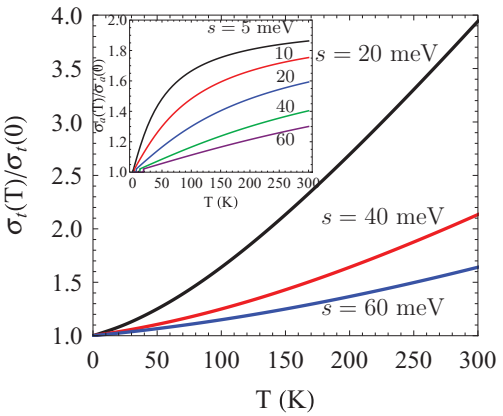

FIG. 7. (Color online) $\sigma_t(T)$ of BLG at charge neutral point for different s [Eq. (22a) with n_e for BLG]. Inset shows the thermally activated conductivity in BLG as a function of temperature, where $\sigma_a(T)/\sigma_a(0) = 1 + e^{\beta^2 s^2/2}\mathrm{erfc}(\beta s/\sqrt{2})$, the same as for the MLG case.

the activated conductivity is weakly temperature dependent except around CNP, i.e., $E_F < s$. Since the density increase by thermal excitation is also suppressed exponentially by the same factor [see Eq. (31)] the dominant temperature-dependent conductivity arises from the scattering mechanism.[1] On the other hand, in the low mobility sample with large value of s, the linear temperature dependence due to thermal activation can be observed even at high carrier densities $E_F \gtrsim s$.

In Fig. 8 we calculate the total conductivities (a) for a fixed E_F and several s and (b) for a fixed s and several E_F. Even for homogeneous BLG, there are two scattering mechanisms competing with each other. The short-range disorder in BLG contributes to a strong insulating transport behavior for all temperatures, whereas screened Coulomb scattering always leads to a metallic behavior for $T \ll T_F$.[35] At the low-temperature limit, the total conductivity $\sigma_t(T)$ decreases with increasing temperature, but at higher temperatures, the short-range disorder contribution becomes quite big and leads to a $\sigma_t(T)$ increasing with T. Therefore, when s is small, the scattering mechanism is dominant and

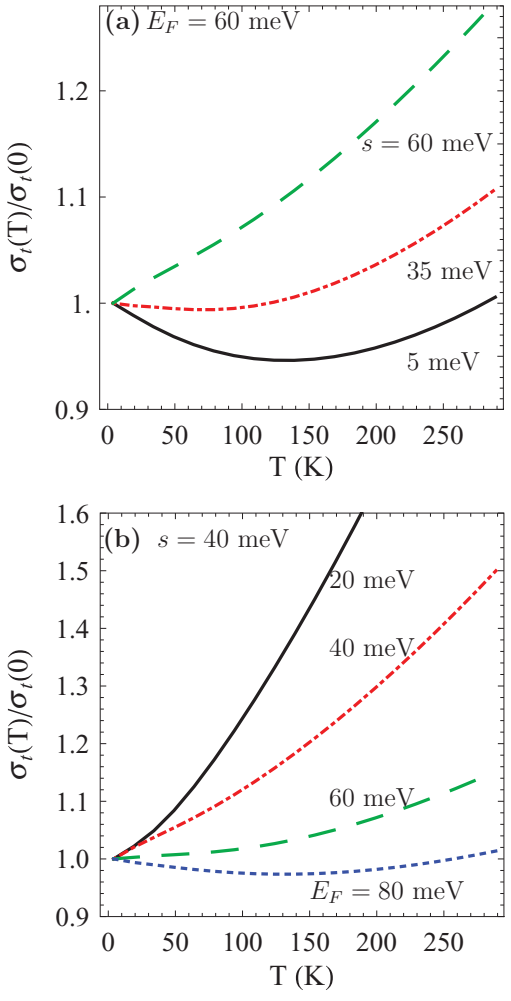

FIG. 8. (Color online) Calculated total conductivity $\sigma_t(T)/\sigma_t(0)$ of BLG with the following parameters: $n_i = 10^{12}$ cm^{-2} and $n_d V_0^2 = 2$ (eV Å)^2. (a) $\sigma_t(T)$ for $E_F = 60$ meV and for different s. (b) $\sigma_t(T)$ for $s = 40$ meV and for several $E_F = 20$, 40, 60, 80 meV, which correspond to the net carrier densities $n = n_e - n_h = 0.55 \times 10^{12}$, 1.1×10^{12}, 1.6×10^{12}, and 2.2×10^{12} cm^{-2}.

the total conductivity manifests a nonmonotonic temperature dependence [see Fig. 8(a)]. However, for large s the activated temperature-dependence behavior overwhelms the metallic temperature dependence, and the system shows insulating behavior [see Fig. 8(b)]. It clearly shows that the insulating behavior in the BLG sample appeared at carrier densities as high as 10^{12} cm^{-2} or higher.

VI. CONNECTION TO EARLIER THEORIES

We have demonstrated theoretically that the observed insulating behavior in temperature-dependent monolayer and bilayer graphene conductivity can be explained by the thermal activation between puddles. There are also other theories which have been elaborated to explain low carrier density graphene transport.[14,35,39] In this section, we establish the bridge to connect our current theory and earlier theories on graphene transport due to the formation of inhomogeneous electron-hole puddles near the charge neutrality point.

The key qualitative difference between our theory and all earlier graphene transport theories is the introduction of the two-component transport model where regular diffusive metallic carrier transport coexists with local activated transport due to activation across potential fluctuations in the puddles. Our theory just explicitly accounts for the inhomogeneous landscape in the system, which earlier theories ignored. This two-component nature of graphene transport, where both metallic and insulating behavior coexist because of the existence of puddles, produces the experimentally observed complex temperature dependence with the low-density behavior being primarily insulatinglike and the high-density behavior being primarily metalliclike.

Two different theories have been developed to study the low-density transport in graphene, where the strong density inhomogeneity is dominated. In Ref. 39 Adam *et al.* qualitatively explained the plateaulike approximate nonuniversal minimum conductivity at low carrier density observed in monolayer graphene samples. The basic idea is to introduce an approximate pinning of the carrier density at $n = n^* \approx n_i$ at low carrier density limits $|n| < |n_i|$, where n_i is an impurity density. The constant minimum conductivity is then given by $\sigma_{\min} \sim \sigma(n = n_i)$ for $n < n_i$. This simple theory for monolayer graphene transport qualitatively explained the existence of conductivity minimum plateau and the extent to which the minimum conductivity is not universal, which was in good agreement with the observed density-dependent conductivity over a wide range of charged impurity densities.[5,6] However, this theory did not take account of the highly heterogeneous structure near the charge neutrality point and the thermally activated conductivity at finite temperatures, which then cannot explain the observed nonmonotonic temperature-dependent transport in low mobility graphene samples.[17]

A more elaborate Thomas-Fermi-Dirac (TFD) theory and an effective-medium approximation (EMT) have been introduced in Refs. 26 and 14 to study the electrical transport properties of disordered monolayer graphene. The ground-state-density landscape $n(\mathbf{r})$ can be obtained within this TFD approach and the resultant electrical transport can be calculated by averaging over disorder realizations and the

effective-medium theory. This theory gives a finite minimum conductivity and is able to explain the crossover of the density-dependent conductivity from the minimum value at the Dirac point to its linear behavior at higher doping. Later, this TFD-EMT theory is also applied to calculate the conductivity of disordered bilayer graphene in Ref. 35. The TFD-EMT technique successfully explains the graphene, both MLG and BLG, transport properties in the theoretically difficult inhomogeneity-dominant regime near the charge neutral point, but this approach fails to explain the temperature dependence of the conductivity for a wide range of temperatures.

In our current model discussed above, we include three effects, the electron-hole structure formation, the thermal activated conductivities and the temperature dependence of screening effects, to explain the temperature-dependent conductivity in both monolayer and bilayer graphene systems. The nonmonotonic temperature-dependent conductivity in graphene systems is then naturally understood from the competition between the thermal activation of charge carriers and the temperature-dependent screening effects. Our transport theory qualitatively explains the observed coexisting metallic and insulating transport behavior in both MLG and BLG systems. For low mobility MLG samples, the dominant role on graphene conductivity switches from the thermally activated transport of inhomogeneous electron-hole puddles to metallic temperature-dependent screening effects, which gives rise to a nonmonotonic behavior from the strong insulating behavior at low temperatures to metallic behavior at high temperatures. On the other hand, another nonmonotonic temperature-dependent transport can be observed in very high mobility bilayer graphene devices, i.e., from metallic behavior at low temperatures due to the screening effects of Coulomb scattering to insulating behavior at high temperatures due to the short-range disorder. The merit of our model is that it is so simple that we could get the asymptotic behavior at low- and high-temperature limits analytically. Moreover, it provides a clear physical picture of the dominant mechanisms at different regimes as discussed above.

VII. DISCUSSIONS AND CONCLUSIONS

We first discuss the similarity and the difference between MLG and BLG transport from the perspective of our transport-theory considerations. We find that both manifest an insulating behavior in $\sigma_t(T)$ for low mobility samples. We also find that both systems could exhibit a nonmonotonic temperature-dependent conductivity for low mobility samples. However, the physical origin for the nonmonotonic temperature dependence is quite different in the two systems: in the MLG the nonmonotonic feature comes from the competition between thermal activation and the metallic screening effects, which leads to $\sigma_t(T)$ first increasing and then decreasing with increasing temperature [see Fig. 4(a)], while for BLG, the competition between short-range insulating scattering and metallic Coulomb screening effects leads to $\sigma_t(T)$ first decreasing and then increasing as temperature increases [see Fig. 8(a)]. Most important quantitative difference between MLG and BLG transport comes from their band dispersions, which leads to much weaker effects of density inhomogeneity in MLG so that the anomalous insulating temperature dependence of $\sigma(T)$ is typically not observed in MLG away from the CNP although the gate voltage dependence of MLG and BLG conductivities are similar.[40,41] The linear Dirac carrier system for MLG leads to linear DOS, which goes to zero at CNP, but the parabolic band dispersion relation in BLG leads to a constant DOS. Due to the difference in the density of states between homogeneous MLG and BLG, the modified DOS in inhomogeneous MLG is increased (see Fig. 1) rather than decreased in inhomogeneous BLG (see Fig. 5). The dimensionless potential fluctuation strength $\tilde{s}$ ($\equiv s/E_F$) is much weaker in MLG than in BLG from simple estimates: $\tilde{s}_{\rm BLG}/\tilde{s}_{\rm MLG} \sim 32/\sqrt{\tilde{n}}$ where $\tilde{n} = n/10^{10}$, and $\tilde{s}_{\rm BLG} \gg \tilde{s}_{\rm MLG}$ up to $n = 10^{13}$ cm^{-2}. Direct calculations[1] show that the self-consistent values of s tend to be much larger in BLG than in MLG for identical impurity disorder. In addition, the qualitatively different DOS leads to much stronger effective short-range scattering in BLG compared with MLG even for the same bare scattering strength. Thus the insulating behavior in $\sigma_t(T)$ will show up at high temperatures even for relatively higher mobility BLG samples (i.e., small s). In contrast, only in very low mobility MLG samples, where s is very large, can the insulating behavior of temperature-dependent resistivity be observed.[9,17] No simple picture would apply to a gapped (Δ_g) BLG system, since four distinct energy scales (s, E_F, k_BT, and Δ_g) will compete and the conceivable temperature dependence depends on their relative values.[2,42,43] Our assumption of BLG quadratic band dispersion is valid only at low ($\lesssim 5 \times 10^{12}$ cm^{-2}) carrier densities, where most of the current transport experiments are carried out. At higher densities the band dispersion is effectively linear and the disorder effects on $\sigma_t(T)$ are weaker.

Before concluding, we emphasize that our theory is physically motivated since puddles are experimental facts in all graphene samples. Puddles automatically imply a two-component nature of transport since both diffusive carriers and activated carriers can, in principle, contribute to transport in the presence of puddles. Of course, the effect of puddles is much stronger at low carrier densities, explaining why insulating (metallic) temperature dependence is more generic at low (high) graphene carrier densities. We emphasize that local carrier activation in puddles is just one of (at least) four different independent transport mechanisms contributing to the temperature-dependent conductivity. The other three are temperature-dependent screening (Ref. 11), phonons (Refs. 22 and 23), and Fermi surface thermal averaging (Refs. 11 and 33). Our theory presented here includes the three electronic mechanisms for temperature dependence: screening, Fermi-surface averaging, and puddle activation. We leave out phonons, which have been considered elsewhere (Refs. 22 and 23) and will simply add to the temperature-dependent resistivity. The weak phonon contribution to graphene resistivity makes it possible for the electronic mechanisms to dominate even at room temperatures, but obviously at high enough temperatures, the system will, except perhaps at the lowest densities around the CNP, manifest metallic temperature dependence with the resistivity increasing with temperature because of phonon scattering. Similarly, the puddle effects dominate low densities and therefore the insulating behavior

will persist to very high temperatures around the zero-density CNP since activation across potential fluctuations are dominant at the CNP. It is gratifying to note that these are precisely the experimental observations. We note that in general the temperature-dependent conductivity of graphene could be very complex since many distinct mechanisms could in principle contribute to the temperature dependence depending on the carrier density, temperature range, and disorder in the system. Inclusion of phonons (at high temperatures) and quantum localization (at low temperatures) effects, which are both neglected in our theory, can only complicate things further. What we have shown in this work is that the low-density conductivity near the CNP is preferentially dominated by density inhomogeneity and thermal carrier activation effects leading to an insulating temperature dependence in the conductivity whereas the high-density conductivity, where the puddles are screened out, is dominated by a metallic conductivity due to temperature-dependent screening effects. This general conclusion is consistent with all experimental observations in both MLG and BLG systems to the best of our knowledge except at very high temperatures where phonon effects would eventually lead to metallic behavior at all densities.

To conclude, we have investigated both MLG and BLG transport in the presence of electron-hole puddles within an analytic statistical theory. Our theory explains the experimentally measured insulating behavior at low temperatures and the consequent nonmonotonic behavior for low mobility samples.[17,20,21] A reasonable quantitative agreement with the experimental data can be obtained by choosing appropriate disorder parameters in our theory (i.e., potential fluctuation and impurity strength) for different samples. We find that the puddle parameter s, defining typical potential fluctuations, to be around 10–80 meV in typical graphene samples as extracted by fitting our theory to existing experimental transport data near the charge neutrality point. These values of potential fluctuations characterizing the graphene charge neutrality point are very consistent with direct numerical calculations of graphene electronic structure in the presence of quenched charged impurities.[1,14,26,35] We also relate our current model to earlier theories using the picture of diffusive transport through disorder-induced electron-hole puddles. Finally, we show the similarity and the quantitative difference between MLG and BLG transport in the presence of puddles.

ACKNOWLEDGMENTS

Q.L. acknowledges helpful discussions with D. S. L. Abergel. The work was supported by ONR-MURI, NRI-NSF-SWAN.

APPENDIX: A SELF-CONSISTENT FORMULATION OF GRAPHENE DENSITY OF STATES IN THE PRESENCE OF INHOMOGENEITY

Below we provide a microscopic theory to calculate self-consistently the electronic density of states in the presence of the potential fluctuations caused by random charged impurities located near graphene/substrate interface, which has been applied to two-dimensional semiconductor based electron-gas systems.[44] This self-consistent approach mainly addresses two problems with the presence of random charged impurities. One is the screening of the long-range Coulomb interactions between the carriers and the charged impurities. The other is the real-space potential fluctuations produced by the random array of charged impurities.

The motivation for this Appendix is twofold: (1) providing a microscopic self-consistent theory of graphene density of states in the presence of puddles; (2) showing that our approximate physically motivated density of states [Eq. (2)] is an excellent approximation to the self-consistent density of states.

1. Monolayer graphene

First, we apply the self-consistent consideration of random charged impurities on the density of states in monolayer graphene.

The simple theory of linear screening gives[44]

$$q_{TF} = \frac{2\pi e^2}{\kappa} D_e(E_F), \tag{A1}$$

where q_{TF} is the Thomas-Fermi screening wave vector, $D_e(E_F)$ is the density of states at the Fermi level, and κ is the dielectric constant ($\kappa \simeq 2.5$ for graphene on SiO_2 substrate).

The screening constant shown in Eq. (A1) enters Poisson's equation for the potential change $\phi(r,z)$ produced by a charge density ρ_{ext} (associated with the charged impurities in the graphene/substrate environment). For a charge Ze (we use $Z \equiv 1$ in the calculation) located at $r \equiv \sqrt{x^2+y^2} = 0$ and $z = z_0 > 0$ (on top of the graphene layer), the additional Coulomb potential satisfies

$$\nabla^2\phi(r,z) - 2q_{TF}g(z)\phi_0(r) = -\frac{4\pi Ze\delta(x)\delta(y)\delta(z-z_0)}{\kappa_0}, \tag{A2}$$

where $\kappa_0 = \kappa_v = 1.0$ in the vacuum ($z > 0$), $\kappa_0 = \kappa_{\text{ins}} = 3.9$ in SiO_2 ($z < 0$), and $\kappa = \frac{\kappa_{\text{ins}}+\kappa_v}{2}$. For graphene, $g(z) = \delta(z)$ is the carrier density distribution normal to the interface and $\phi_0(r) = \int \phi(r,z)g(z)dz = \phi(r,0)$.

To solve Eq. (A2) we take advantage of the cylindrical symmetry to write[45]

$$\phi(r,z) = \int_0^\infty J_0(k'r)A_{k'}(z)k'dk'. \tag{A3}$$

The potential will satisfy Eq. (A2) if

$$\frac{d^2A_k}{dz^2} - k^2A_k - 2q_{TF}A_k(0)g(z) = -\frac{2Ze\delta(z-z_0)}{\kappa_0}. \tag{A4}$$

At the interface $z = 0$, $A_k(z)$ must be continuous and satisfy $\kappa_v(dA_k/dz) - \kappa_{\text{ins}}(dA_k/dz) = 2q_{TF}A_k(0)\kappa$. $A_k(z)$ should also satisfy the boundary condition $A_k(z) \to 0$ as $z \to \infty$. In addition, the impurity potential ϕ will go to zero at the metallic contact below the SiO_2 [i.e., $A_k(-d) \equiv 0$ and d is the thickness of the SiO_2 layer]. Such screening effects are absent in the SiO_2. After some algebra, the explicit expression

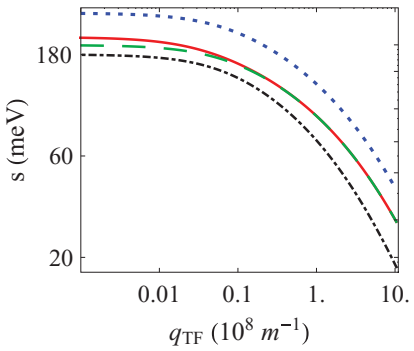

FIG. 9. (Color online) Standard deviation of potential fluctuation s versus the screening constant q_{TF} (log-log plot) in MLG by varying the Fermi level. The dotted blue line is for $n_{\rm imp} = 1.0 \times 10^{12}$ cm^{-2}, $z_0 = 1$ nm, and $d = 100$ nm. The solid red line is for $n_{\rm imp} = 0.5 \times 10^{12}$ cm^{-2}, $z_0 = 1$ nm, and $d = 200$ nm. The dashed green line is for $n_{\rm imp} = 0.5 \times 10^{12}$ cm^{-2}, $z_0 = 1$ nm and $d = 100$ nm. The dot-dashed black line is for $n_{\rm imp} = 0.5 \times 10^{12}$ cm^{-2}, $z_0 = 2$ nm and $d = 100$ nm.

of $A_k(k,0)$ for insulator thickness d and the impurity distance from graphene/substrate interface z_0 is given by

$$A_k(k,0) = \frac{2e^{-kz_0} Ze \sinh(dk)}{k\kappa_{\rm ins}\cosh(dk) + (k\kappa_v + 2q_{TF}\kappa)\sinh(dk)}. \quad \text{(A5)}$$

For the thickness of insulator in the limit $d \to \infty$, we have $A_k(k,0) = \frac{e^{-kz_0} Ze}{(k+q_{TF})\kappa}$, which has been given in Appendix B of Ref. 45. The potential fluctuations with an array of point charges at random positions in the plane $z = z_0$ have a mean-square variation about the average potential ,[44]

$$V_{\rm rms}^2 = 2\pi n_{\rm imp} e^2 \int [A_k(0)]^2 k dk. \quad \text{(A6)}$$

To obtain specific results for the electronic density of states and the screening constant we use the simple Gaussian broadening approximation for the density of states.[27] The disorder-induced potential-energy fluctuations are described by $P(V) = \frac{1}{\sqrt{2\pi s^2}} \exp(-V^2/2s^2)$ [Eq. (A6)]. Then the density of states becomes

$$D_e(E) = \int_{-\infty}^{E} \frac{g_s g_v (E - V)}{2\pi(\hbar v_F)^2} P(V) dV$$
$$= D_1 \left[\frac{E}{2} \text{erfc}\left(-\frac{E}{\sqrt{2}s} \right) + \frac{s}{\sqrt{2\pi}} \exp\left(-\frac{E^2}{2s^2} \right) \right], \quad \text{(A7)}$$

where erfc(x) is the complementary error function, $s = V_{\rm rms}$, $D_1 = \frac{g_s g_v}{2\pi(\hbar v_F)^2}$, v_F is the graphene (Fermi) velocity, $g_s = 2$ and $g_v = 2$ are the spin and valley degeneracies, respectively.

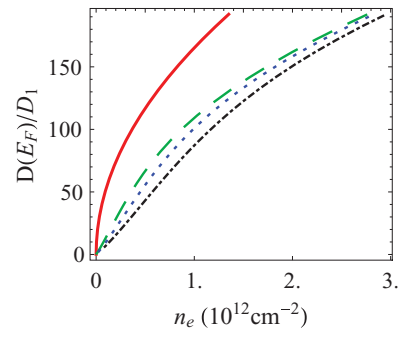

FIG. 10. (Color online) Calculated the density of states of electron $D_e(E_F)$ in MLG versus electron density using the following parameters: the insulator thickness $d = 100$ nm, the impurity distance from the interface $z_0 = 1$ nm. The solid red line is for unperturbed density of states. The dashed green, dotted blue, and dot-dashed black lines correspond to $n_{\rm imp} = 0.5$, 1.0, and 2.0×10^{12} cm^{-2}, respectively.

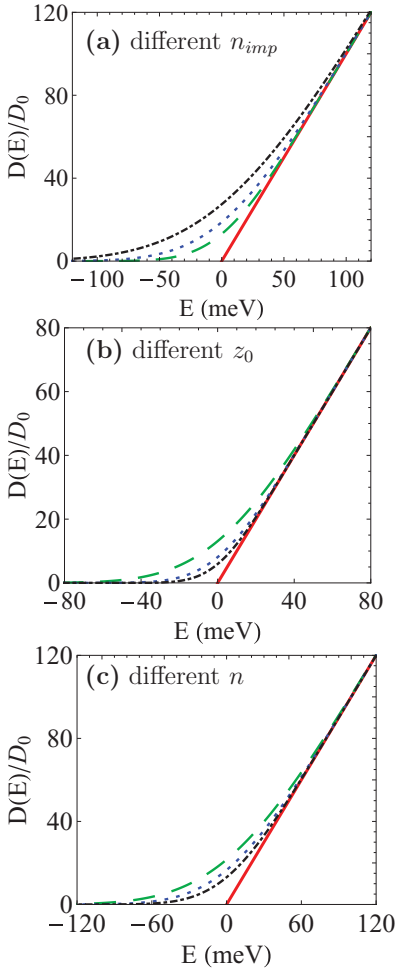

FIG. 11. (Color online) Calculated density of states of electron $D_e(E)$ of MLG versus energy E for different impurity configurations and carrier densities n. The solid red lines are for the noninteracting MLG system. (a) Calculated $D_e(E)$ in MLG for the insulator thickness $d = 100$ nm, the impurity distance from the interface $z_0 = 1$ nm, and carrier density $n = 2.0 \times 10^{12}$ cm^{-2}. The dashed green, dotted blue, and dot-dashed black lines correspond to $n_{\rm imp} = 0.5$, 1.0, 2.0×10^{12} cm^{-2}, respectively. (b) Calculated $D_e(E)$ in MLG for $d = 100$ nm, $n_{\rm imp} = 0.5 \times 10^{12}$ cm^{-2}, and $n = 2.0 \times 10^{12}$ cm^{-2}. The dashed green, dotted blue, and dot-dashed black lines correspond to $z_0 = 1$, 2, 3 nm, respectively. (c) Calculated $D_e(E)$ in MLG for $d = 100$ nm, $z_0 = 1$ nm, and $n_{\rm imp} = 0.5 \times 10^{12}$ cm^{-2}. The dashed green, dotted blue, and dot-dashed black lines correspond to $n = 0.5$, 1.0, 2.0×10^{12} cm^{-2}, respectively.

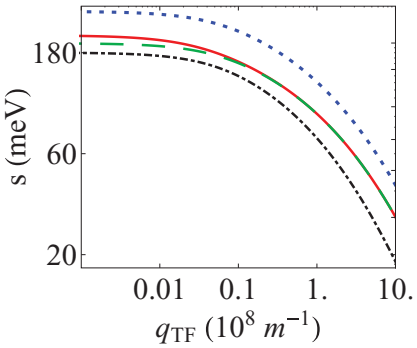

FIG. 12. (Color online) Standard deviation of potential fluctuation s versus the screening constant q_{TF} (log-log plot) in BLG by varying the Fermi level. The dotted blue line is for $n_{imp} = 1.0 \times 10^{12}$ cm^{-2}, $z_0 = 1$ nm and $d = 100$ nm. The solid red line is for $n_{imp} = 0.5 \times 10^{12}$ cm^{-2}, $z_0 = 1$ nm, and $d = 200$ nm. The dashed green line is for $n_{imp} = 0.5 \times 10^{12}$ cm^{-2}, $z_0 = 1$ nm, and $d = 100$ nm. The dot-dashed black line is for $n_{imp} = 0.5 \times 10^{12}$ cm^{-2}, $z_0 = 2$ nm, and $d = 100$ nm.

By choosing the chemical potential E_F as a tuning parameter we have the following coupled equations:

$$q_{TF} = \frac{2\pi e^2}{\kappa} D_e(E_F),$$
$$s^2 = 2\pi n_{imp} e^2 \int [A_k(0)]^2 k dk. \quad \text{(A8)}$$

For fixed values of E_F, n_{imp}, d, and z_0, we get the self-consistent results for s, q_{TF} by solving the above two coupled equations. The electron density could be gotten from the formula

$$n_e = \int_{-\infty}^{\infty} D_e(\epsilon) f(\epsilon) d\epsilon, \quad \text{(A9)}$$

where $f(\epsilon)$ is the Fermi-Dirac distribution function. The electron density in the presence of disorder-induced electron-hole puddles has been discussed in Sec. II, where we use the potential fluctuation s as a fixed parameter. And here we self-consistently solve the parameter s from a microscopic point of view, which is in good agreement with the results shown in Sec. II. The potential fluctuation in Eq. (A6) affects the electronic density of states. But the fluctuations depend on the screening via Eq. (A4) while the screening depends on the density of states via Eq. (A1). Therefore we have a coupled problem that must be solved self-consistently.

In Fig. 9, the standard deviation of the potential fluctuation s and the screening constant q_{TF} are plotted for different values of the Fermi level. The self-consistently solved parameters (s, q_{TF}) depend on the fixed charged impurity density n_{imp}, the SiO_2 thickness d, the location of the fixed charged impurity z_0, and the Fermi level E_F (i.e., the carrier density n). All four

FIG. 13. (Color online) Calculated density of states of electron $D_e(E_F)$ of BLG versus electron density using the following parameters: the insulator thickness $d = 100$ nm, the impurity distance from the interface $z_0 = 1$ nm. The solid red line is for unperturbed density of states. The dashed green, dotted blue, and dot-dashed black lines correspond to $n_{imp} = 0.5$, 1.0, and 2.0×10^{12} cm^{-2}, respectively.

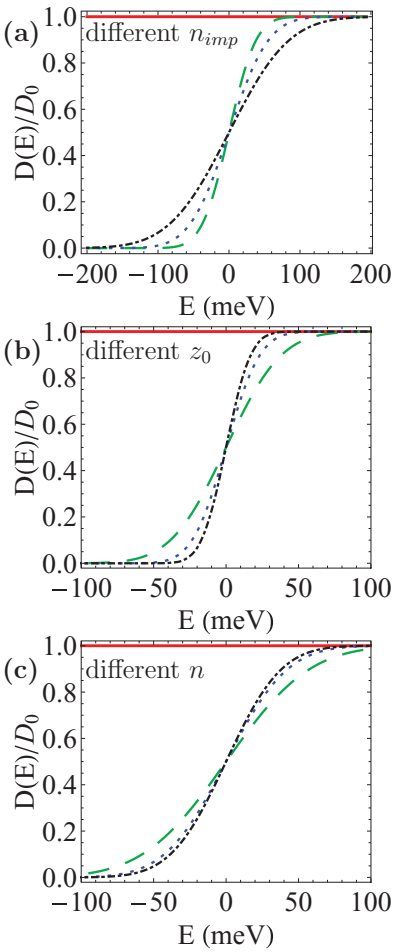

FIG. 14. (Color online) Calculated density of states of electron $D_e(E)$ of BLG versus energy E for different impurity configuration and carrier densities n. The solid red lines are for the noninteracting BLG system. (a) Calculated $D_e(E)$ in BLG for the insulator thickness $d = 100$ nm, the impurity distance from the interface $z_0 = 1$ nm, and carrier density $n = 2.0 \times 10^{12}$ cm^{-2}. The dashed green, dotted blue, and dot-dashed black lines correspond to $n_{imp} = 0.5$, 1.0, 2.0×10^{12} cm^{-2}, respectively. (b) Calculated $D_e(E)$ in BLG for $d = 100$ nm, $n_{imp} = 0.5 \times 10^{12}$ cm^{-2}, and $n = 2.0 \times 10^{12}$ cm^{-2}. The dashed green, dotted blue, and dot-dashed black lines correspond to $z_0 = 1$, 2, 3 nm, respectively. (c) Calculated $D_e(E)$ in BLG for $d = 100$ nm, $z_0 = 1$ nm, and $n_{imp} = 0.5 \times 10^{12}$ cm^{-2}. The dashed green, dotted blue, and dot-dashed black lines correspond to $n = 0.5$, 1.0, 2.0×10^{12} cm^{-2}, respectively.

of these effects can be understood from physical intuition. The reduction of the SiO_2 thickness weakens the potential fluctuations when the screening length is small even though there is a little effect for strong screening. As the charged impurities go away from the graphene layer the potential fluctuations is also reduced, while the potential fluctuations become stronger with the higher impurity density. Increasing the carrier density n gives rise to the stronger screening effects, and leads to weaker potential fluctuations.

In Fig. 10, the density of states of monolayer graphene is given with the parameters of SiO_2 thickness $d = 100$ nm and the distance of fixed charged impurities $z_0 = 1$ nm for different impurity densities $n_{\rm imp}$. In Fig. 11, we present the electronic density of states for different carrier densities and impurity configurations. The self-consistent calculation of the density of states verifies the results presented in Sec. II as shown in Fig. 1, where we choose the potential fluctuation s as an adjustable parameter. For monolayer graphene, the presence of spatially random charged impurities increases the electronic density of states in the whole range of energy. The corresponding hole density of states can be obtained by changing the sign of energy $D_h(E) = D_e(-E)$.

2. Bilayer graphene

In this subsection, we provide the density of states in bilayer graphene in the presence of potential fluctuations. As shown for monolayer graphene, we use the linear screening written as[44]

$$q_{TF} = \frac{2\pi e^2}{\kappa} D_e(E_F), \tag{A10}$$

where $D_e(E_F)$ is the density of states of BLG at the Fermi level and κ is the dielectric constant and for BLG on SiO_2, $\kappa \simeq 2.5$.

Following the same procedure discussed for MLG, the disorder-induced potential fluctuation is described by the Gaussian form $P(V) = \frac{1}{\sqrt{2\pi s^2}} \exp(-V^2/2s^2)$ and the corresponding density of states can be written as (also see Sec. IV)

$$D_e(E) = \int_{-\infty}^{E} \frac{g_s g_v m}{2\pi\hbar^2} P(V) dV = \frac{D_0}{2} \mathrm{erfc}\left(-\frac{E}{\sqrt{2}s}\right), \tag{A11}$$

where $\mathrm{erfc}(x)$ is the complementary error function, $s = V_{\rm rms}$ [as given in Eq. (A6)], $D_0 = \frac{g_s g_v m}{2\pi\hbar^2}$, $g_s = 2$, and $g_v = 2$ are the spin and valley degeneracies, respectively. The main difference between MLG and BLG is in their density of states of noninteracting systems. The homogeneous MLG system has the linear energy-dependent density of states while the density of states of the homogeneous BLG is independent of energy, which leads to different Thomas-Fermi screening wave vectors. The potential fluctuation in Eq. (A6) affects the electronic density of states in BLG, but the fluctuations depend on the screening via Eq. (A4) while the screening depends on the density of states via Eq. (A10). Therefore we have a coupled problem that must be solved self-consistently.

In Fig. 12, the broadening parameter s and the screening constant q_{TF} are plotted for various Fermi levels (i.e., the carrier density n). As shown for MLG, the BLG parameters (s, q_{TF}) are also a nontrivial function of the fixed charge density $n_{\rm imp}$, the SiO_2 thickness d, the location of the fixed charged impurity z_0, and the Fermi level. The different charged impurity configurations and carrier densities have similar effects on potential fluctuations of bilayer graphene as we discussed for monolayer graphene. The results for $s(q_{TF})$ are also quite similar to that of MLG (in Fig. 9) only with a small numerical difference.

In Fig. 13, the self-consistent electronic density of states of BLG has been calculated using SiO_2 thickness $d = 100$ nm and distance of fixed charged impurities $z_0 = 1$ nm for different impurity densities. The higher impurity density changes the density of states more dramatically. In Fig. 14, we show the electronic density of states of BLG for different charged impurity configurations and carrier densities. The existence of random charged impurities reduces the electronic density of states for $E > 0$ but creates a band tail for $E < 0$.

[1] S. Das Sarma, S. Adam, E. H. Hwang, and E. Rossi, Rev. Mod. Phys. **83**, 407 (2011).

[2] E. V. Castro, K. S. Novoselov, S. V. Morozov, N. M. R. Peres, J. M. B. Lopes dos Santos, J. Nilsson, F. Guinea, A. K. Geim, and A. H. Castro Neto, Phys. Rev. Lett. **99**, 216802 (2007).

[3] Y. Lee, S. Bae, H. Jang, S. Jang, S.-E. Zhu, S. H. Sim, Y. I. Song, B. H. Hong, and J.-H. Ahn, Nano Lett. **10**, 490 (2010).

[4] K. S. Novoselov, D. Jiang, F. Schedin, T. J. Booth, V. V. Khotkevich, S. V. Morozov, and A. K. Geim, Proc. Natl. Acad. Sci. USA **102**, 10451 (2005); K. S. Novoselov, A. K. Geim, S. V. Morozov, D. Jiang, M. I. Katsnelson, I. V. Grigorieva, S. V. Dubonos, and A. A. Firsov, Nature (London) **438**, 197 (2005).

[5] Y.-W. Tan, Y. Zhang, K. Bolotin, Y. Zhao, S. Adam, E. H. Hwang, S. Das Sarma, H. L. Stormer, and P. Kim, Phys. Rev. Lett. **99**, 246803 (2007).

[6] J. H. Chen, C. Jang, S. Adam, M. Fuhrer, E. D. Williams, and M. Ishigami, Nat. Phys. **4**, 377 (2008).

[7] X. Hong, K. Zou, and J. Zhu, Phys. Rev. B **80**, 241415 (2009).

[8] F. Chen, J. Xia, and N. Tao, Nano Lett. **9**, 1621 (2009).

[9] Y.-W. Tan, Y. Zhang, H. Stormer, and P. Kim, Eur. Phys. J. Special Top. **148**, 15 (2007).

[10] J. H. Chen, C. Jang, S. Xiao, M. Ishigami, and M. S. Fuhrer, Nat. Nanotechnol. **3**, 206 (2008).

[11] E. H. Hwang and S. Das Sarma, Phys. Rev. B **79**, 165404 (2009).

[12] M. Lv and S. Wan, Phys. Rev. B **81**, 195409 (2010).

[13] E. H. Hwang, S. Adam, and S. Das Sarma, Phys. Rev. Lett. **98**, 186806 (2007).

[14] E. Rossi, S. Adam, and S. Das Sarma, Phys. Rev. B **79**, 245423 (2009).

[15] J. Martin, N. Akerman, G. Ulbricht, T. Lohmann, J. H. Smet, K. V. Klitzing, and A. Yacoby, Nat. Phys. **4**, 144 (2008).

[16]Y. Zhang, V. W. Brar, C. Girit, A. Zettl, and M. F. Crommie, Nat. Phys. **5**, 722 (2009); A. Deshpande, W. Bao, F. Miao, C. N. Lau, and B. J. LeRoy, Phys. Rev. B **79**, 205411 (2009); A. Deshpande, W. Bao, Z. Zhao, C. N. Lau, and B. J. LeRoy, *ibid*. **83**, 155409 (2011).

[17]J. Heo, H. J. Chung, S.-H. Lee, H. Yang, D. H. Seo, J. K. Shin, U. In Chung, S. Seo, E. H. Hwang, and S. Das Sarma, Phys. Rev. B **84**, 035421 (2011).

[18]W. Zhu, V. Perebeinos, M. Freitag, and P. Avouris, Phys. Rev. B **80**, 235402 (2009).

[19]B. Feldman, J. Martin, and A. Yacoby, Nat. Phys. **5**, 889 (2009).

[20]K. Zou and J. Zhu, Phys. Rev. B **82**, 081407 (2010).

[21]S.-G. Nam, D.-K. Ki, and H.-J. Lee, Phys. Rev. B **82**, 245416 (2010).

[22]E. H. Hwang and S. Das Sarma, Phys. Rev. B **77**, 115449 (2008).

[23]H. Min, E. H. Hwang, and S. Das Sarma, Phys. Rev. B **83**, 161404 (2011).

[24]E. H. Hwang and S. Das Sarma, Phys. Rev. B **82**, 081409 (2010).

[25]D. S. L. Abergel, E. H. Hwang, and S. Das Sarma, Phys. Rev. B **83**, 085429 (2011).

[26]E. Rossi and S. Das Sarma, Phys. Rev. Lett. **101**, 166803 (2008).

[27]E. Arnold, Appl. Phys. Lett. **25**, 705 (1974).

[28]P. San-Jose, E. Prada, and D. S. Golubev, Phys. Rev. B **76**, 195445 (2007); J. H. Bardarson, J. Tworzydło, P. W. Brouwer, and C. W. J. Beenakker, Phys. Rev. Lett. **99**, 106801 (2007); E. Louis, J. A. Vergés, F. Guinea, and G. Chiappe, Phys. Rev. B **75**, 085440 (2007).

[29]R. Zallen and H. Scher, Phys. Rev. B **4**, 4471 (1971).

[30]T. P. Eggarter and M. H. Cohen, Phys. Rev. Lett. **25**, 807 (1970).

[31]X. Du, I. Skachko, A. Barker, and E. Y. Andrei, Nat. Nanotech. **3**, 491 (2008).

[32]K. I. Bolotin, K. J. Sikes, J. Hone, H. L. Stormer, and P. Kim, Phys. Rev. Lett. **101**, 096802 (2008).

[33]M. Müller, M. Bräuninger, and B. Trauzettel, Phys. Rev. Lett. **103**, 196801 (2009).

[34]S. Kirkpatrick, Rev. Mod. Phys. **45**, 574 (1973).

[35]S. Das Sarma, E. H. Hwang, and E. Rossi, Phys. Rev. B **81**, 161407 (2010).

[36]E. H. Hwang and S. Das Sarma, Phys. Rev. B **75**, 205418 (2007).

[37]A. Ferreira, J. Viana-Gomes, J. Nilsson, E. R. Mucciolo, N. M. R. Peres, and A. H. Castro Neto, Phys. Rev. B **83**, 165402 (2011).

[38]E. H. Hwang and S. Das Sarma, Phys. Rev. Lett. **101**, 156802 (2008).

[39]S. Adam, E. H. Hwang, V. M. Galitski, and S. Das Sarma, Proc. Natl. Acad. Sci. USA **104**, 18392 (2007).

[40]S. V. Morozov, K. S. Novoselov, M. I. Katsnelson, F. Schedin, D. C. Elias, J. A. Jaszczak, and A. K. Geim, Phys. Rev. Lett. **100**, 016602 (2008).

[41]S. Xiao, J.-H. Chen, S. Adam, E. D. Williams, and M. S. Fuhrer, Phys. Rev. B **82**, 041406 (2010).

[42]J. B. Oostinga, H. B. Heersche, X. Liu, A. F. Morpurgo, and L. M. K. Vandersypen, Nat. Mater. **7**, 151 (2008).

[43]K. F. Mak, C. H. Lui, J. Shan, and T. F. Heinz, Phys. Rev. Lett. **102**, 256405 (2009).

[44]F. Stern, Surf. Sci. **58**, 162 (1976).

[45]F. Stern and W. E. Howard, Phys. Rev. **163**, 816 (1967).